Magnetic ordering and spin-reorientation transitions in $TbCo_3B_2$

Moshe Dubman*
Nuclear Research Centre—Negev, P.O. Box 9001, Beer-Sheva 84190, Israel
and Department of Physics, Ben-Gurion University, P.O. Box 653, Beer-Sheva 84105, Israel

El'ad N. Caspi and Hanania Ettedgui
Nuclear Research Centre—Negev, P.O. Box 9001, Beer-Sheva 84190, Israel

Lukas Keller
Laboratory for Neutron Scattering, ETH Zürich and Paul Scherrer Institute, CH-5232 Villigen PSI, Switzerland

Mordechai Melamud†
Israel Atomic Energy Commission, P.O. Box 7061, Tel Aviv 61070, Israel

Hagai Shaked
Department of Physics, Ben-Gurion University, P.O. Box 653, Beer-Sheva 84105, Israel
(Received 28 February 2005; published 21 July 2005)

The magnetic structure of the compound $TbCo_3B_2$ has been studied in the temperature range 1.5 K$\leqslant T \leqslant$300 K by means of neutron powder diffraction, magnetization, magnetic ac susceptibility, and heat capacity measurements. The compound is of hexagonal symmetry and is paramagnetic at 300 K, undergoes a magnetic Co-Co ordering transition at ~170 K, and a second magnetic Tb-Tb ordering transition at ~30 K. The latter induces a spin-reorientation transition, in which the magnetic axis rotates from the c axis toward the basal plane. Below this transition a symmetry decrease (γ magnetostriction) sets in, leading to an orthorhombic distortion of the crystal lattice. The crystal and magnetic structures and interactions and their evolution with temperature are discussed using a microscopic physical model.

DOI: 10.1103/PhysRevB.72.024446 PACS number(s): 75.50.Cc, 61.12.Ld, 75.30.Gw, 75.30.Et

I. INTRODUCTION

The ternary intermetallic compounds of the $R_{n+1}Co_{3n+5}B_{2n}$ (R=lanthanide; n=0, 1, 2, 3, ∞) family crystallize with a unique structural regularity as a function of n (Fig. 1). These structures belong to the $P6/mmm$ space group.[1] Over the past decades, this family served as a fertile ground for many theoretical and experimental investigations, where emphasis had been put on the Co-rich compounds such as $SmCo_5$.[2] This is owing to their technological importance as permanent magnetic materials, as they combine a very high magnetic anisotropy energy density with a high T_C (~1000 K).[2] The RCo_5 (n=0) compounds are isostructural to RCo_3B_2 (n=∞, Fig. 1) and have an interesting magnetic behavior. They order ferromagnetically (light R) and ferrimagnetically (heavy R) with the magnetic axis along the c axis. At a characteristic lower temperature, some undergo a spin reorientation transition (SRT), where the magnetic axis rotates toward the plane perpendicular to the c axis. This transition is linked with an increase of the magnetic moment of R, μ_R. We show in the present work that $TbCo_3B_2$ qualitatively replicates this behavior, albeit, remarkable quantitative differences, for example, a change in temperature scale.

The compound $TbCo_3B_2$ (n=∞) is studied in the present work by means of neutron powder diffraction (NPD), magnetic ac susceptibility, heat capacity (HC), x-ray powder diffraction (XRD), and magnetization measurements. This compound was previously studied using a sample of lesser quality and low statistics NPD.[3,4] Our interest in this compound arises from the fact that although isostructural with $TbCo_5$ (Fig. 1), the replacement of two Co atoms (site 2c) by B atoms, drastically alters its magnetic properties. For example, the value of T_C, and the magnetic moments of both Tb and Co (μ_{Tb} and μ_{Co}) are considerably smaller in $TbCo_3B_2$. In the present study we attempt to shed light on the reasons for the above differences, and on questions left unanswered in previous studies, in particular the origin of the 170 K anomaly observed in the ac susceptibility.[3]

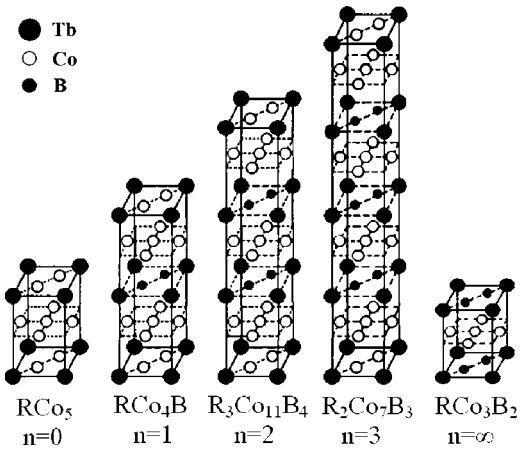

FIG. 1. Crystal structure of the compounds in the $R_{n+1}Co_{3n+5}B_{2n}$ (R=lanthanide; n=0,1,2,3,∞) family. RCo_3B_2 is obtained from RCo_5 by replacing the Co at the 2c site by B (Ref. 1).

II. SAMPLE PREPARATION, CHARACTERIZATION, AND EXPERIMENTAL METHODS

A $TbCo_3B_2$ sample ($\sim$18 g) was synthesized at the Nuclear Research Centre—Negev (NRCN) using ^{11}B-enriched (99.95%) boron in order to reduce sample thermal neutron absorption. Initially the CoB precursor was prepared by arc melting of the constituents in an argon atmosphere. The ingot was then remelted several times to increase homogeneousness, annealed, and analyzed using Cuk_α XRD. The CoB ingot was found to contain less than 1 w/o of an unidentified impurity phase. The $TbCo_3B_2$ sample was synthesized by arc melting of the CoB precursor along with elemental Co and Tb in order to achieve stoichiometry. The $TbCo_3B_2$ ingot was remelted several times and subsequently annealed at 1073 °C for 120 h. The annealed sample was characterized by XRD at the NRCN as $TbCo_3B_2$ ($CeCo_3B_2$-type structure[5]) plus two minor ($<2\%$) lines of an unidentified phase.

Measurements of ac susceptibility were carried out at the NRCN using a home made ac susceptometer, with operating frequency of 1.5 kHz. The magnitude of the alternating magnetic field was $\sim$10 Oe, and the data were collected in the temperature range 9 K–296 K. The $TbCo_3B_2$ specimen used for ac-susceptibility measurements weighed 124 mg and was taken from the sample used for the NPD measurements.

The dc magnetic measurements were performed using a quantum design superconducting quantum interference device (SQUID) magnetometer (model MPMS5), at the Racah Institute of Physics—the Hebrew University in Jerusalem. The dependence of the magnetization on temperature was measured in the temperature range 4 K–250 K, with an applied and cooling field of about 60 Oe. Magnetization versus magnetic field curves, $M(H)$, were measured for -10 kOe $\leqslant H \leqslant 50$ kOe at several temperatures in the range 5 K–250 K. These were taken in the following manner: the initial magnetization curve at each temperature was taken up to 50 kOe, and then the sample was demagnetized by reversing the field down to -10 kOe. All SQUID data have been collected using a 20 mg specimen taken from the powder sample that was used for the NPD measurements.

HC measurements at constant pressure in the temperature range 5 K–200 K were carried out using a quantum design instrument, model PPMS, located at the Paul Scherrer Institute (PSI). The 24 mg specimen used in the HC measurement was taken from the powder sample that was used for the NPD measurements.

NPD measurements were carried out on a ground sample using the high resolution powder diffractometer for thermal neutrons (HRPT) instrument,[6] located at PSI, set to the high-intensity mode, with a neutron wavelength of $\lambda = 1.8857$ Å. The sample was loaded into a liquid-He-cooled cryostat, and measured at various temperatures in the range 1.5 K–220 K. The obtained diffraction profiles were analyzed with the Rietveld refinement technique using the FULLPROF program.[7]

III. RESULTS OF MACROSCOPIC MEASUREMENTS

A. ac susceptibility and magnetization versus temperature (Fig. 2)

The ac susceptibility and the zero field cooling (ZFC) and field cooling (FC) magnetization of $TbCo_3B_2$ as a function of temperature are shown in Fig. 2. The sharp decrease in χ and M/H upon heating at $T_{SRT} = 30(3)$ K are due to a decrease in the magnitude of μ_{Tb}, which is related to a SRT that $TbCo_3B_2$ undergoes at this temperature (Sec. IV). A maximum at 170 (15) K in the ac-susceptibility data and the merging of the ZFC and FC magnetization curves close to this temperature are evident. We propose that these features correspond to a transition to a magnetic order at $T_C = 170(15)$ K. In previous works, 30 K was identified as the Curie temperature of $TbCo_3B_2$,[3,8] considerably lower than T_C of the present work. The ac susceptibility of $TbCo_3B_2$ for $T > T_C$ markedly deviates from the Curie-Weiss law, as one would expect for the case of a ferrimagnet.[9]

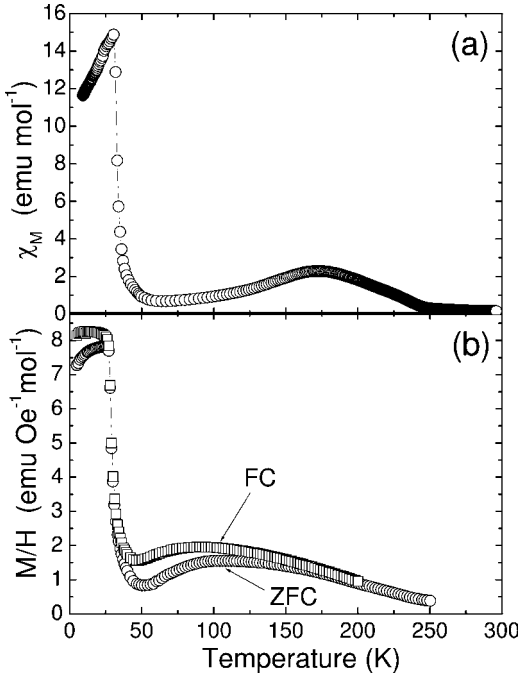

FIG. 2. Molar ac-susceptibility (a) and SQUID-magnetization data (b) of $TbCo_3B_2$ as a function of temperature. The applied magnetic field during the ZFC and FC data collecting and FC cooldown is $H \sim 60$ Oe.

B. Magnetization versus magnetic field (Figs. 3 and 4)

The initial magnetization curves of $TbCo_3B_2$ at several temperatures are shown in Fig. 3(a). The saturation magnetization at 5 K is $M_{sat}(5\text{ K}) = 6.2(1)\mu_B$/f.u. [119(5) emu/g], and the extrapolated zero field magnetization is $M_{H=0}(5\text{ K}) = 4.9(2)\mu_B$/f.u. [94(3) emu/g]. These values support the existence of ferro/ferri- magnetic ordering at this temperature. A comparison between the present initial magnetization curve at 5 K (Fig. 3) and a similar curve given in Ref. 8 shows an agreement in the $M_{H=0}(5\text{ K})$ values. In both curves, the magnetization is not fully saturated at 50 kOe. However, the value of $M_{sat}(5\text{ K})$ reported in Ref. 8 is greater by $\sim 1.5\ \mu_B$. The dependence of $M_{H=0}(T)$ on temperature is shown in Fig. 3(b).

Partial hysteresis loops taken in the manner described in Sec. II for $T = 40$, 80, 130, and 250 K, are shown in Fig. 4(a).

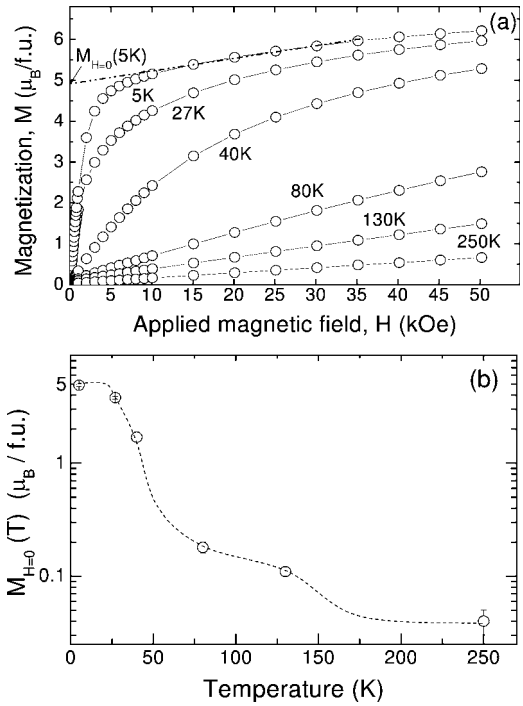

FIG. 3. (a) Initial magnetization curves of $TbCo_3B_2$ at various temperatures. (b) Semilog $M_{H=0}(T)$ values, as extrapolated from the curves depicted in (a). The dotted line serves as a guide to the eye. The $M_{H=0}(T)$ values were obtained in the following manner: for each temperature, $M_{H=0}(T)$ is the intersection between the axis and a straight line. The straight line is calculated by a least-square fit of the raw data points in the region 10 kOe$\leqslant H \leqslant$35 kOe.

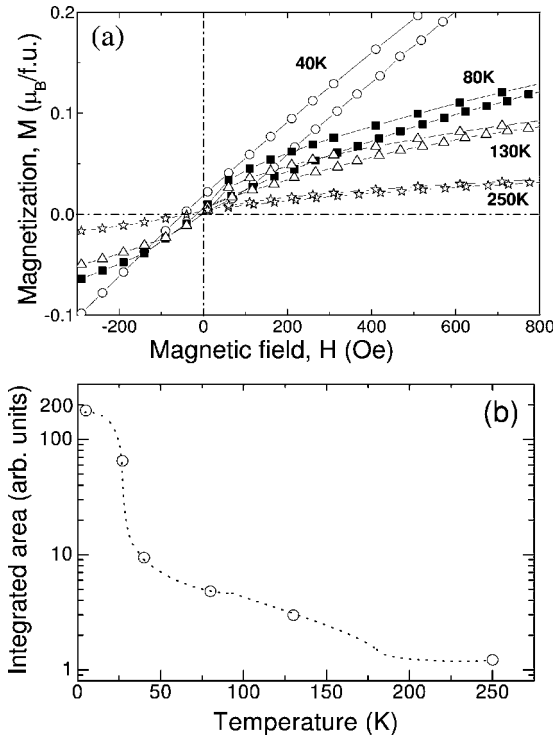

FIG. 4. (a) Partial hysteresis loops for $TbCo_3B_2$ at various temperatures. (b) Semilog integrated area values, confined within the loops at 20 Oe$<H<$1.5 kOe. The dependence of the areas on temperature show a decrease of magnetic order with increasing temperature. The data for 250 K is virtually a straight line with neglible amounts of hysteresis, indicating that at this temperature the sample is paramagnetic. The dotted line serves as a guide to the eye.

7The areas confined within the loops in the range 20 Oe–1500 Oe, are shown on a semilogarithmic scale in Fig. 4(b).

By inspection of the hysteresis areas and the values of $M_{H=0}(T)$ (Figs. 3(b) and 4(b)), it is evident that although very subtle, the magnetic order in $TbCo_3B_2$ does not vanish with the sharp decrease of magnetization at 30 K. It is nonzero above 30 K, persists up to 130 K, and seems to vanish somewhere between 150 and 250 K. This is in support of the magnetization and ac-susceptibility results (Sec. III A, Fig. 2), which suggest $T_C \sim 170$ K.

C. Heat capacity (Fig. 5)

The measured molar HC of $TbCo_3B_2$ (the present work) is depicted in Fig. 5(a), along with a published measurement on YCo_3B_2.[10] An anomaly is observed for $TbCo_3B_2$ at ~30 K, which is absent for YCo_3B_2. In Fig. 5(b), the difference between the two curves is shown. We note that Y^{3+} is nonmagnetic and YCo_3B_2 is isostructural with $TbCo_3B_2$. Thus, assuming that the curve shown in Fig. 5(b) is a good approximation for the magnetic contribution to the HC of $TbCo_3B_2$, the feature, which appears in Fig. 5(b) at 30 K, must be due to a magnetic phase transition related to the Tb^{3+} ion at this temperature. The existence of a magnetic phase transition at this temperature is consistent with the macroscopic magnetic measurements (Figs. 2–4).

Above the transition temperature, the magnetic contribution to the heat capacity does not vanish but rather slightly increases. In order to find out at which temperature this contribution would vanish, another experiment should be conducted on YCo_3B_2 at a broader temperature range. However, a transition in the vicinity of T_C does not appear in the HC data, probably since at such elevated temperatures the phonon and other contributions dominate the weaker magnetic ones.

The result given in Fig. 5 is similar, quantitatively and qualitatively, to published results for RCo_3B_2 with R=Gd, Sm, Dy.[10] In addition, the dependence of the magnetic part of C_P near 30 K is similar to the dependence reported for another family of permanent magnets, $R_2T_{14}B_2$ near their SRT temperature.[11]

IV. NEUTRON DIFFRACTION RESULTS AND ANALYSIS

The $TbCo_3B_2$ sample was studied at 16 different temperatures in the range 1.5 K$\leqslant T \leqslant$220 K.[12] At each temperature, a set of NPD data was collected and analyzed by the Rietveld refinement technique to obtain the structural and magnetic parameters that best fit these data (Fig. 6). An inspection of the collected data, renders, prior to the Rietveld analysis, invaluable information regarding the sample's crystal and magnetic structures, and leads to the following preliminary

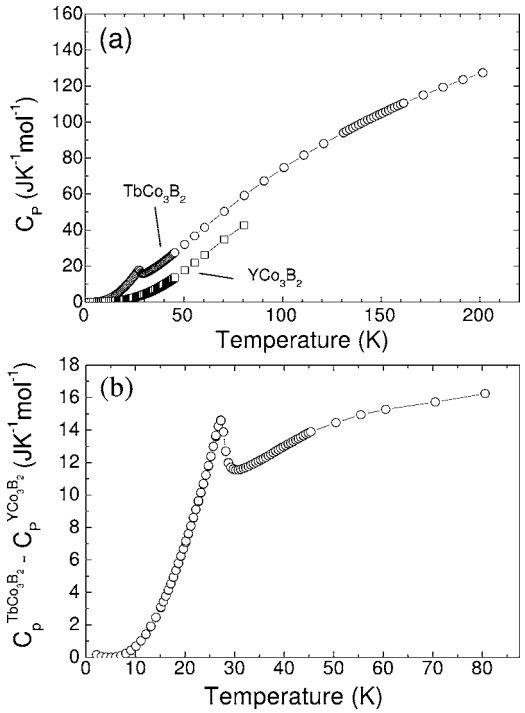

FIG. 5. (a) Total molar heat capacity of $TbCo_3B_2$ (circles, 24 mg sample, present work) and of YCo_3B_2 (squares, Ref. 10). (b) Magnetic contribution to the molar heat capacity of $TbCo_3B_2$, calculated by subtracting the YCo_3B_2 from $TbCo_3B_2$ of (a).

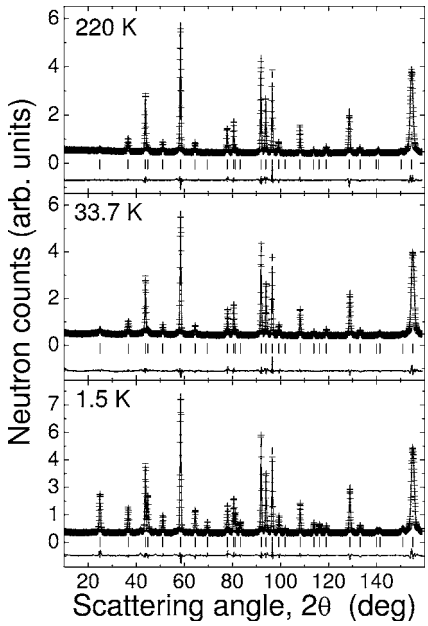

FIG. 6. Rietveld refinement profiles for $TbCo_3B_2$ at 220, 33.7, and 1.5 K. The plus signs are the raw powder diffraction data, the solid line is the calculated (refined) profile, and the solid line at the bottom is the difference between the observed and calculated profiles. The tick marks below the diffraction profile represent the positions of Bragg reflections. The diffraction profiles are normalized for statistics. The emergence of extra intensities at Bragg positions at 1.5 K indicates a ferro-ferrimagnetic order at this temperature.

finding: (i) The NPD profiles exhibit a considerable intensity increase of some Bragg reflections with a sample temperature decrease (e.g., at scattering angles 25°, 46°, 70°; Fig. 6). This intensity increase is due to ferro-/ferrimagnetic order developing with the decrease of sample's temperature (consistent with the results of the macroscopic measurements; Sec. III). (ii) The magnetic contribution to {100} and {001} at $T<30$ K (Fig. 7) requires a magnetic axis component perpendicular to [001] (basal plane component). Whereas the magnetic contribution to {100}, with the absence of a magnetic contribution to {001} at $T>30$ K, requires a magnetic axis component along [001] (axial component), and excludes any basal plane component. This indicates that the transition at 30 K is indeed a SRT, where, upon cooling, the magnetic axis rotates from the axial direction toward the basal plane. (iii) A careful examination of the NPD profiles at $T<30$ K reveals a subtle but statistically significant broadening of reflections with $h,k\neq 0$ (e.g., {100}, {110}, {220}), with no observable broadening of reflections with $h=k=0$ (e.g., {001}, {002}). This selective broadening is consistent with a crystal symmetry reduction at the SRT. Such a reduction is indeed required from magnetic symmetry considerations at $T<T_{SRT}$, as a basal plane component in a ferro-/ferrimagnetic structure is inconsistent with the $P6/mmm$ crystallographic space group.[13] The space group Cmmm, which allows this component, is a maximal subgroup of $P6/mmm$.[1]

In view of the preliminary findings, eight alternative models (Table I) were studied in the Rietveld refinement of the NPD data. The input to the Rietveld refinement contained the crystallographic parameters (with the space group specified by the model) in the first phase and the magnetic structure in the second phase. For all models, all nonmagnetic parameters (e.g., Atomic positions, peak shape, FWHM, etc.) were constrained to be equal among the two phases. Rietveld refinements of several models (Table I) were performed with the dataset of each temperature. The models that best fit the datasets show, upon cooling, the para-, axial, and canted magnetic phases, in agreement with the NPD preliminary findings and with the results of the macroscopic measurements (Sec. III). The proposed magnetic structures of the present work (Table II, Fig. 8) consist of these best-fit models. In choosing the best-fit models, there were cases where the quality of the fit (agreement factors) of the best-fit model was only slightly better than another relevant model. In these cases, we used the method of comparison between two models, devised by Prince.[14] The Prince test shows that at $T<T_{SRT}$, the better agreement of model IV over models III and V (Table I) to the NPD data is statistically significant, with a confidence level of 99.99%. For the 12 datasets taken at 33.7 K$\leqslant T\leqslant$149 K, when comparing models II and VI (Table I), the Prince test for each dataset do not show a preference for any model. However, since out of the 12 datasets not a single dataset gives a better fit to model VI, we reject this model, and accept model II (Table I, Fig. 8). Refinements of μ_{Co} and μ_{Tb} to fit the 220 K data could not be made to converge. Hence, the $\chi^2(\mu_{Co},\mu_{Tb})$ surface was calculated over a grid in the μ_{Co}-μ_{Tb} plane. The surface showed a definite minimum at $\mu_{Co}\sim\mu_{Tb}\sim 0$, rendering no magnetic order at 220 K.

The refined crystallographic and magnetic parameters for the best-fit models are listed for selected temperatures in

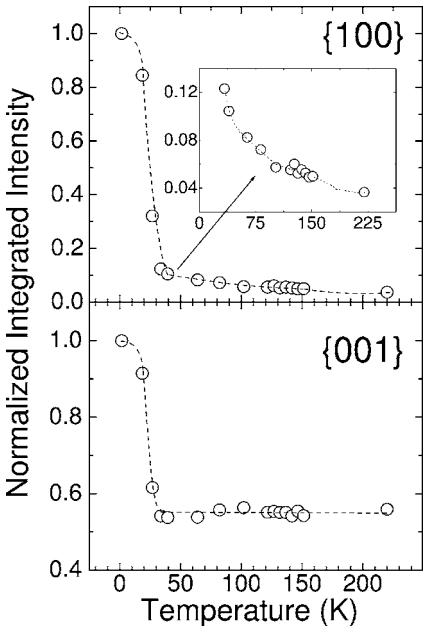

FIG. 7. Normalized integrated intensities of the {100} and {001} reflections (at $2\theta \approx 25°$ and 37° in Fig. 7, respectively) as a function of temperature. The dashed lines serve as guides to the eye. Notice that {001} has a magnetic contribution only for $T < 30$ K, but no magnetic contribution at higher temperatures, where {100} still has some contributions. This indicates that the spin axis is along [001] at these temperatures.

Table III. The $P6/mmm$ lattice parameters, c and a, decrease monotonically as the sample is cooled down to 30 K (Fig. 9). Below 30 K, where the orthorhombic distortion takes place, c increases and the hexagonal a splits into two values $(a_0/\sqrt{3}, b_0)$, where a_0 and b_0 are the orthorhombic Cmmm lattice parameters (Fig. 8). In refining the canted magnetic structure (model IV, $T < 30$ K), the magnetic axis was assumed to be in the a_0c plane, as the NPD data could not provide any information regarding the azimuthal angle of the magnetic axis.[15] That is, $(\mu_x, 0, \mu_z)$ was refined for μ_{Tb} and for μ_{Co}.

TABLE II. Models (Table I) used in the final Rietveld analysis of the data taken at different temperatures. The values of T_{SRT} and T_C are 30(3) K and 170(15) K, respectively.

Temperature	Model
$T > T_C$	I
$T_{SRT} < T < T_C$	II
$T < T_{SRT}$	IV

The NPD-refined values of the magnetic moments in the selected models are given in Fig. 10. The refined magnetic moment per formula unit (fu) at 1.5 K is equal to (Table III): $\mu_{Tb}\text{-}3\cdot\mu_{Co}=5.2(2)\ \mu_B\text{-}3\cdot 0.12(2)\ \mu_B=4.8(2)\mu_B$/f.u. and is in good agreement with the value of $M_{H=0}(5\text{ K})=4.9(2)\ \mu_B$/f.u., obtained from the magnetization measurements. This agreement corroborates the proposed ferrimagnetic model (Sec. III A).

V. DISCUSSION

The magnetic structure of $TbCo_3B_2$ has been studied, in the present work, in the temperature range 1.5 K–220 K. NPD, magnetic ac susceptibility, magnetization, and specific heat measurements, were used in this study. It is found that $TbCo_3B_2$ is paramagnetic at 220 K. Upon cooling, a ferrimagnetic order sets in at $T_C \sim 170(15)$K, in which each of the sublattices (Tb and Co) orders ferromagnetically, but are coupled antiferromagnetically to each other (Fig. 8). The magnetic axis of this ferrimagnet is along the c axis. Upon further cooling, at $T_{SRT} \sim 30$ K, the magnetic axis rotates

TABLE I. Models (Mod) of magnetic structures with their crystal structures, that were refined using the NPD data of the present work. Agreement factors for the refinements of these models at two selected temperatures are given. The agreement factors of the best fit models are given in bold.

			Agreement factors (%)					
			1.5 K			**33.7 K**		
Mod	Description of the magnetic structure	Crystal space group	R_p	R_{Bragg}	R_{wp}	R_p	R_{Bragg}	R_{wp}
I	Paramagnetic	$P6/mmm$	7.97	16.47	14.60	3.06	4.36	4.12
II	Collinear$\parallel c$ axis	$P6/mmm$	5.20	9.24	8.75	**2.99**	**4.08**	**3.93**
III	Collinear$\perp c$ axis	Cmmm	3.36	3.67	4.55		No convergence	
IV	Collinear canted[a]	Cmmm[b]	**3.32**	**3.46**	**4.47**		No convergence	
V	μ_{Tb} canted, $\mu_{Co}=0$	Cmmm	3.36	3.59	4.52		No convergence	
VI	$\mu_{Tb}\parallel c$, $\mu_{Co}=0$	$P6/mmm$	5.20	9.27	8.75	3.00	4.18	3.94
VII	$\mu_{Tb}\perp c$, $\mu_{Co}\parallel c$	Cmmm	3.42	3.90	4.64		No convergence	
VIII	$\mu_{Tb}\parallel c$, $\mu_{Co}\perp c$	$P6/mmm$[c]	4.79	7.96	8.08		No convergence	

[a]θ_μ has been fit as an additional parameter and the refined value is $\theta_\mu=74(2)°$.
[b]With crystal space group $P6/mmm$, agreement factors 3.42%, 3.62%, and 4.60% for R_P, R_{Bragg}, and R_{wp}, respectively, are obtained.
[c]At 1.5 K, the same model in Cmmm does not converge.

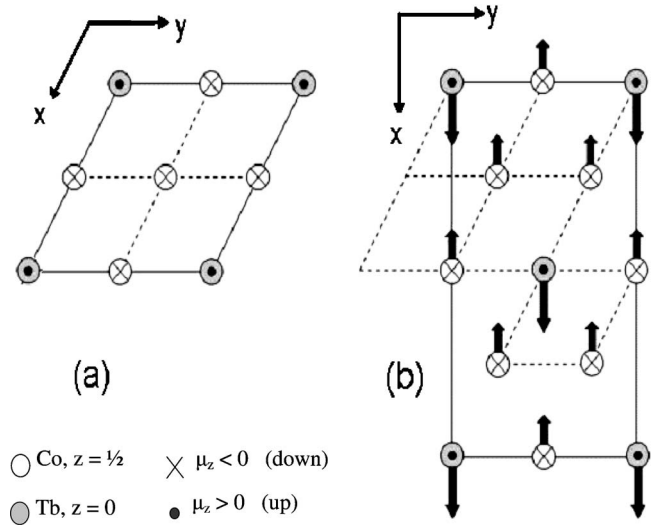

FIG. 8. Schematics of the proposed ferrimagnetic structures. (a) The high symmetry (hexagonal), high temperature ($30\ \mathrm{K} < T < T_C$) structure. The magnetic axis is along the z axis (model II). (b) The low-symmetry (orthohexagonal), low-temperature ($1.5\ \mathrm{K} < T < 30\ \mathrm{K}$) structure. The magnetic axis is canted at an angle θ_μ from the z axis, so that $(\mu_x/\mu_z)_{\mathrm{Tb}} = (\mu_x/\mu_z)_{\mathrm{Co}} = \tan(\theta_\mu)$ (model IV).

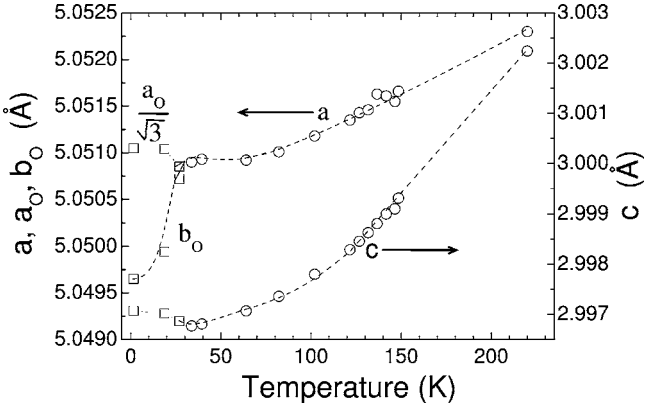

FIG. 9. Lattice parameters versus temperature. a_O and b_O were refined in the C*mmm* representation (Fig. 8), whereas a was refined in the *P*6/*mmm* representation. When the orthorhombic distortion vanishes, $b_O = a_O/\sqrt{3} = a$. The dashed lines serve as guides to the eye. Statistical errors are smaller than the symbols and are not shown.

from the c axis toward the plane perpendicular to the c axis. This SRT is accompanied by a sharp increase of the magnitude of μ_{Tb}, but not that of μ_{Co} (Fig. 10), and by the onset of an orthorhombic distortion of the basal plane (Fig. 9).

The present ac-susceptibility data show a broad peak centered at ~170 K (Fig. 2), $M(T)$ data show separation of the ZFC and FC curves at ~185 K (Fig. 2), $M(H)$ data show the disappearance of hysteresis losses somewhere in the region $130\ \mathrm{K} < T < 250\ \mathrm{K}$ (Fig. 4), and no magnetic order was observed by means of NPD at 220 K. All of the above is consistent with $T_C = 170(15)\mathrm{K}$ in this compound.

In ions of the light and heavy lanthanides, the spin and magnetic moment are parallel and antiparallel to each other, respectively (Hund's third rule). Experimental data show that the magnetic moments in the R and Co sublattices in the RCo_5 (and RCo_4B) system are parallel and antiparallel to each other for the light and heavy lanthanides, respectively.[2,16] This is since, in these systems, the R-Co coupling is dominated by the spin-spin exchange interaction. The proposed magnetic structure of $TbCo_3B_2$ at $T < T_C$ concurs with the above rule, indicating that also in $TbCo_3B_2$ it is the exchange between the Co and Tb spins that determines

TABLE III. Refined values of structural and magnetic parameters of $TbCo_3B_2$, at 5 selected (out of 16) temperatures. Rietveld refinements of the 220 and 33.7 K data were performed in the hexagonal *P*6/*mmm* space group, and of the 1.5, 18.6, and 26.9 K data, in the orthorhombic C*mmm* space group (Fig. 8) (Ref. 1). Atom positions in the hexagonal space group are Tb(0,0,0), Co$(\frac{1}{2},0,\frac{1}{2})$, and B$(\frac{2}{3},\frac{1}{3},0)$ (sites 1a, 3g, 2b, repectively); and in the orthorhombic space group Tb(0,0,0), Co1$(\frac{1}{2},0,\frac{1}{2})$, Co2$(\frac{1}{4},\frac{1}{4},\frac{1}{2})$, and B$(x,0,0)$ (Ref. 1). The magnetic parameters θ_μ, μ_{Tb}, and μ_{Co} were refined with the magnetic axis in the a_O–c plane (Fig. 8). B_{Tb}, B_{Co}, and B_{B} are the isotropic thermal factors. A sample absorption coefficient of $\mu R = 1.56$ was measured and used in the refinements. Numbers in parentheses are the estimated standard deviations (esd) of the refined values. Where esd values are absent, the parameter was not refined.

T (K)	1.5	18.6	26.9	33.7	220
a_O (Å)	8.7487(5)	8.7487(6)	8.7484(4)		
a (Å)				5.0509(2)	5.0523(2)
b_O (Å)	5.0496(3)	5.0499(4)	5.0508(3)		
c (Å)	2.9971(1)	2.9970(1)	2.9969(1)	2.9968(1)	3.0022(1)
x	0.667(3)	0.667(5)	0.667(1)		
B_{Tb} (Å^2)	1.01(1)	0.97(3)	0.93(3)	0.86(3)	1.11(3)
B_{Co} (Å^2)	0.68(2)	0.68(3)	0.71(3)	0.73(3)	0.82(2)
B_{B} (Å^2)	1.15(2)	1.15(2)	1.15(2)	1.14(3)	1.30(2)
μ_{Tb} (μ_{B})	5.2(1)	4.8(1)	2.5(4)	0.9(1)	0
μ_{Co} (μ_{B})	−0.12(2)	−0.09(2)	−0.15(3)	−0.21(11)	0
θ_μ (°)	74(2)	75(1)	49(3)	0	0

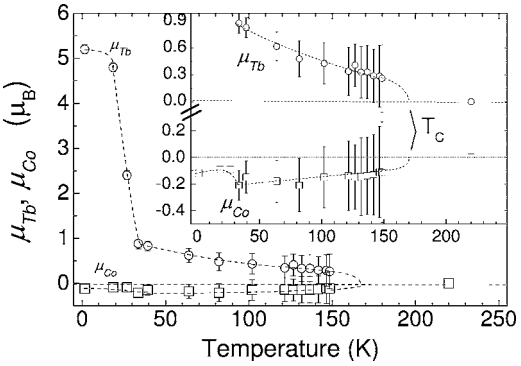

FIG. 10. The refined values of the magnetic moments of Tb (circles), μ_{Tb}, and of Co (squares), μ_{Co}, versus temperature. The dashed lines serve as guides to the eye. At 220 K, $\mu_{\mathrm{Co}} \sim \mu_{\mathrm{Tb}} \sim 0$ were deduced from a minimum in the χ^2 surface (Sec. IV).

the relative orientation of the moments between the sublattices and leads to the ferrimagnetic structure.

In the isostructural $R\mathrm{Co}_5$ system, many magnetic properties such as the magnitude of μ_R at the lowest temperature (LT) and the value of T_{SRT} can be calculated from the solutions of the Hamiltonian:[17]

$$H = K_1^R \sin^2 \theta_\mu + K_1^T \sin^2 \theta_\mu + g\mu_B \, \mathbf{J} \cdot \mathbf{H_M}, \qquad (1)$$

where θ_μ is the angle between the magnetic and the unique axes (colinearity is assumed), $\mathbf{H_M}$ is the exchange field at the R ion site, μ_{B} is the Bohr magneton, and g and $\mathbf{J}$ are the Landé factor and the total angular momentum of the trivalent R ion, respectively. The superscripts R and T represent the rare earth and transition metal ions (R and Co in $R\mathrm{Co}_5$), respectively.

The first and second terms in Eq. (1) represent the magnetocrystalline anisotropy energy contribution from the R and Co sites, respectively (in units of energy density), and the third term represents the interaction of the rare earth moment with the exchange field that originates mainly from Co-Co exchange, neglecting Tb-Tb exchange (for $R\mathrm{Co}_5$).

A general calculation of K_1^T is very difficult, due to the unlocalized character of the $3d$ electrons of Co. On the other hand, as the $4f$ magnetic electrons have a much more localized character, K_1^R could be estimated through[18]

$$K_1^R \propto -\frac{3}{2} \mathrm{B}_2^0 \langle O_2^0 \rangle, \qquad (2)$$

where $\mathrm{B}_2^0 O_2^0$ is the first term in the expansion of the crystalline electric field (CEF) interaction within Stevens' operator equivalent Hamiltonian formalism.[19] $\langle O_2^0 \rangle$ is the thermal average of the first-order Stevens operator, $\mathbf{O}_2^0 = 3\mathbf{J}_z^2 - \mathbf{J}(\mathbf{J}+1)$, and B_2^0 is the second-order crystal field parameter,[17]

$$\mathrm{B}_2^0 = \alpha_J \langle r_{4f}^2 \rangle A_2^0, \qquad (3)$$

where α_J and $\langle r_{4f}^2 \rangle$ are the Stevens multiplicative factor and the effective squared spatial span of the electron cloud, which depend solely on the $4f$ ion under investigation (e.g., Ref. 17), while A_2^0 depends mainly on the crystal structure of the compound.

For $R_{n+1}\mathrm{Co}_{3n+5}\mathrm{B}_{2n}$, one can state a "rule of thumb," according to which A_2^0 (Eq. (3)) becomes more negative when n increases, hence enhancing the CEF effects. This can be understood within the point-charge-model expression for A_2^0 (see, for instance, Ref. 20), in which the in-plane and out-of-plane neighbors contribute positively and negatively to A_2^0, respectively. Hence, when going from TbCo_5 ($n=0$) to $\mathrm{TbCo}_3\mathrm{B}_2$ ($n=\infty$), the replacement of the in-plane Co ions by negatively charged B ions decreases positive contributions,[21] and the shortening of the c-axis further increases negative contributions. For example, in the $\mathrm{Sm}_{n+1}\mathrm{Co}_{3n+5}\mathrm{B}_{2n}$ system, Mössbauer spectroscopy measurements show that A_2^0 changes from -698 to -2203 K Å^2 when n changes from 0 to ∞, respectively.[21]

The magnetic structures and their temperature evolution proposed in the present work could be in a first stage qualitatively described by the $R\mathrm{Co}_5$ Hamiltonian (Eq. (1)). However, a more accurate treatment will possibly require additional terms, such as a Tb-Tb exchange term (see later). Upon cooling, the Co sublattice spontaneously orders ferromagnetically at $T_{\mathrm{C}} \sim 170$ K. This ordering is driven by the Co-Co exchange and the magnetic axis is along the c axis. This order induces, through the exchange term (third term) in Eq. (1), a ferromagnetic order of a small component of μ_{Tb} on the Tb sublattice. The Co and Tb sublattices are coupled antiferromagnetically, as expected of Tb (heavy R). To concur with the axial magnetic order (experimentally found in the present work), it is stipulated that $K_1^T > 0$. As in $R\mathrm{Co}_5$, it is expected that K_1^T is approximately independent of temperature.[17] Below T_{C}, at T close to T_{C}, the ordered component of μ_{Tb} (i.e. $\langle J_z^2 \rangle$, see above) is small, leading to a small value of K_1^R and the K_1^T term in Eq. (1) dominates. As the temperature is decreased, the ordered component ($\langle J_z^2 \rangle$) increases (insert, Fig. 10), leading to an increase in the magnitude of K_1^R, but keeping $K_1^T + K_1^R$ positive. At $\sim$30 K, an ordering transition driven by the Tb-Tb exchange sets in on the Tb sublattice, leading to a sharp increase in the ordered component of μ_{Tb} (i.e., $\langle J_z^2 \rangle$), hence, making the first term sharply more negative. At this temperature, $K_1^T + K_1^R$ becomes negative, leading to the SRT (i.e., sending $\theta_\mu = 0$ to $\theta_\mu = \pi/2$). This model (Eq. (1)) can only have two solutions for $\theta_\mu (= 0, \pi/2)$ and cannot explain the experimental result of canted magnetic axis ($\theta_\mu = 74^\circ$). To explain the experimental result of canted magnetic axis, one needs to introduce an additional term with the next order anisotropy constant, say $K_2^R \sin^4 \theta_\mu$, to the Hamiltonian.

Magnetic transitions at $T_{\mathrm{C}} \sim 170$ K were also observed in $\mathrm{Tb}_{0.75}\mathrm{U}_{0.25}\mathrm{Co}_3\mathrm{B}_2$,[22] $\mathrm{CeCo}_3\mathrm{B}_2$,[23] $\mathrm{HoCo}_3\mathrm{B}_2$,[24] and $Y\mathrm{Co}_3\mathrm{B}_2$.[25] Evidently, this transition is present in $R\mathrm{Co}_3\mathrm{B}_2$, independent of R. Moreover, it exists for diamagnetic $R(=Y)$, corroborating our proposition that it is Co-Co exchange driven. In the course of the SRT, μ_{Co} decreases slightly, whereas μ_{Tb} increases sharply. For $R\mathrm{Co}_5$ with R=Tb, Ho, Dy, which undergo SRT at a characteristic temperature, a decrease in μ_{Co} and an increase in μ_R during SRT are also observed. However, in $\mathrm{TbCo}_3\mathrm{B}_2$ the increase in μ_R is much more prominent (the increase in TbCo_5 is only $\sim$10%).[26] This is consistent with our proposal that the SRT in $\mathrm{TbCo}_3\mathrm{B}_2$ is driven by onset of Tb-Tb ordering (due to presumably RKKY exchange)

TABLE IV. Selected magnetic and crystallographic properties of $TbCo_3B_2$ (present work), and $TbCo_5$. Magnetic moments are given at 1.5 K and 4 K for $TbCo_3B_2$ and $TbCo_5$, respectively. Cell parameters are given at 220 K and room temperature for $TbCo_3B_2$ and $TbCo_5$, respectively.

Property		$TbCo_3B_2$	$TbCo_5$
T_C	(K)	170(15)	984[42]
T_{SRT}	(K)	30(3)	400[42]
μ_{Tb}	(μ_B)	5.2(1)	8.5[28]
μ_{Co} (3g)	(μ_B)	−0.12(2)	−1.7[26]
μ_{Co} (2c)	(μ_B)	⋯	−1.5[26]
$\lambda^{\gamma,2}$	(10^{-4})	3.0(2)	$\leqslant 1$[33]
a	(Å)	5.0523(2)	5.050(3)[5]
c	(Å)	3.0022(1)	4.009(2)[5]

transition. No such transition exists in $TbCo_5$, where μ_{Tb}, which is near saturation, increases slowly, exhibiting a small and a broad change at the SRT. We have no explanation for the small decrease in μ_{Co} at the SRT, in both systems.

Experimental[26] and theoretical[20,27] studies of RCo_5 show that the magnitude of the ordered R magnetic moment at LT is close to its free-ion value (for $TbCo_5$, $\mu_{Tb}=8.5\ \mu_B$,[28] compared to the free-ion value of 9 μ_B, Table IV). However, for $TbCo_3B_2$, the present NPD data show that $\mu_{Tb}(\mathrm{LT})=5.2(1)\ \mu_B$ (Table III), which is significantly lower than the free-ion value. The NPD data of $HoCo_3B_2$ show $\mu_{Ho}(4\ \mathrm{K})=5\ \mu_B$,[24] half of the free Ho-ion value. A similar result was deduced from macroscopic measurements on $DyCo_3B_2$, $\mu_{Dy}(\mathrm{LT})\sim 7.6\ \mu_B$,[29] compared to a free-ion value of Dy $\sim 10\ \mu_B$. That is, when going from RCo_5 ($n=0$) to RCo_3B_2 ($n=\infty$), the ordered R-sublattice magnetic moment at LT decreases significantly. This is due to the increase of CEF with n, and is consistent with the above "rule of thumb". In addition, canting of the magnetic axis with respect to the unique crystal axis typically appears in systems with non-negligible CEF-driven anisotropy such as RCo_5 and $R_2Fe_{14}B$,[30,31] whereas in systems such as R_2T_{17} and RT_2M_2 (T—transition metal), in which exchange interactions (third term, Eq. (1)) dominate, such canting is not common. The hexagonal $TbCo_3B_2$ undergoes an orthorhombic distortion (Figs. 8 and 9) for $T<T_{SRT}$, whose magnitude reaches $2.8(2)\times 10^{-4}$ at 1.5 K (Table III). The corresponding γ-magnetostriction constant, $\lambda^{\gamma,2}$, is equal to $3.0(2)\cdot 10^{-4}$.[32] No orthorhombic distortion was detected (XRD) in any of the RCo_5 compounds,[33] and for $TbCo_5$ it was estimated[33] that $\lambda^{\gamma,2}\leqslant 10^{-4}$ (Table IV). The larger γ magnetostriction in $TbCo_3B_2$ as compared to $TbCo_5$ is more evidence for the stronger anisotropy in $TbCo_3B_2$.

It has been well established, that, for $R_{n+1}Co_{3n+5}B_{2n}$, the Co magnetic moment, μ_{Co}, decreases with an increase of n, that is, when the number of average neighboring B-containing planes increases.[3,16,34] For example, for $TbCo_5$, $\mu_{Co}(3g)\sim 1.7\ \mu_B$, while for $TbCo_3B_2$, $\mu_{Co}(3g)\sim 0.12\ \mu_B$. This is related with the increase of the average distance between two neighboring Co-containing planes (i.e., ~2 Å for $TbCo_5$, and ~3 Å for $TbCo_3B_2$), along with hybridization of the Co($3d$) orbitals with the nonmagnetic B($2p$) orbitals,[35–37] both lead to a decrease in $\mathbf{H_M}$ (the exchange term in Eq. (1)). This weakening of the exchange as one goes from $TbCo_5$ to $TbCo_3B_2$ also leads to the decrease in T_C and T_{SRT} (Table IV).

In $TbCo_3B_2$, where the contribution to K_1^T (Eq. (1)) comes from a single Co site, the $3g$ site (Fig. 1, Table III), we have found that K_1^T, namely $K_1^{(3g)}$, is positive. On the other hand, in the isostructural RCo_5 it was found that $K_1^{(3g)}$ is negative, however, $K_1^T(=2K_1^{(2c)}+3K_1^{(3g)})$ is positive.[17,38–40] The $3g$ Co_3 layer is sandwiched between a pair of $TbCo_2$ and TbB_2 and TbB_2 layers, in $TbCo_5$ and $TbCo_3B_2$, respectively (Fig. 1). Hence, it is the replacement of Co_2 by B_2 in the pair of $TbCo_2$ layers that changes the sign of $K_1^{(3g)}$ from negative in $TbCo_5$ to positive in $TbCo_3B_2$. Furthermore, it was found experimentally in $R_{n+1}Co_{3n+5}B_{2n}$ ($R=Y$, La; $n=1$, 2, 3),[41] that the contribution to K_1^T from a Co_3 layer is negative whenever sandwiched between a pair of RCo_2 layers, and is otherwise positive. Hence, present results extend the above result to the $n=\infty$ case.

VI. SUMMARY

$TbCo_3B_2$ is hexagonal and paramagnetic at room temperature. Upon cooling, it undergoes a first magnetic-ordering phase transition at $T_C\sim 170$ K, driven by the Co-Co exchange. Below T_C, the c-aligned ferromagnetic Co and Tb sublattices are coupled antiferromagnetically. At $T_{SRT}\sim 30$ K, the Tb-Tb exchange drives a second phase transition, leading to a sharp increase of μ_{Tb}. This increase leads to a sharp increase in the single-ion anisotropy energy of the Tb ion, and, correspondingly, in the crystalline magnetostrictive energy. Consequently, below T_{SRT}, the magnetic axis is canted away from the c axis (i.e., spin-reorientation transition), and the crystal lattice is orthorhombically distorted.

This behavior replicates, though on a significantly lower-temperature scale, the magnetic behavior of the isostructural $TbCo_5$. The replacement of Co_2 by B_2 in the $TbCo_3B_2$ structure leads to the following (Table IV): (i) A decrease in the Co-Co exchange due to an increase in the Co-Co distance. (ii) A decrease in μ_{Co} due to B($2p$) and Co($3d$) hybridization. (iii) The contribution to K_1^T from the $Co^{(3g)}$ site changes from negative to positive. (iv) An increase in the magnetocrystalline anisotropy energy due to an increase in CEF. (v) A decrease in μ_{Tb} due to an increase in CEF. The decreases in the Co-Co exchange and in μ_{Co} are responsible for the decrease in T_C. Consequently, μ_{Tb} remains small down to the temperature, where the ordering transition of the Tb sublattice takes place, where it increases sufficiently to drive the spin-reorientation transition. The increase in the magnetocrystalline energy is responsible for the larger magnetostriction, and the observed orthorhombic distortion.

These effects are not unique for the Tb ion. A low T_C has already been observed in several other RCo_3B_2 compounds and solid solutions, and it is expected that RCo_3B_2 will replicate, with the above differences, the magnetic behavior of their corresponding RCo_5 compounds, for all R.

ACKNOWLEDGMENTS

This work is partly based on the experiments performed at the Swiss Spallation Neutron Source—SINQ, Paul Scherrer Institute, Villigen, Switzerland. The authors express their gratitude to Denis Sheptyakov, the HRPT instrument responsible, and to Israel Felner from the Racah Institute of Physics—Hebrew University of Jerusalem, for his help with the SQUID measurements, taken at his laboratory.

---

*Corresponding author: Moshe Dubman, Nuclear Research Centre—Negev, P. O. Box 9001, Beer-Sheva IL-84190, Israel. Telephone: +972-8-6567876; fax: +972-8-6567878; electronic address: dovman54@netvision.net.il

†Present address: CTBTO, Vienna International Center, P.O. Box 1200, Vienna 1400, Austria.

[1] T. Hahn, in *International Tables for Crystallography* (Reidel, Dordrecht, 1983) Vol. A.

[2] E. A. Nesbitt and J. H. Wernick, *Rare Earth Permanent Magnets* (Academic, New York, 1973).

[3] E. N. Caspi, H. Pinto, M. Kuznietz, H. Ettedgui, M. Melamud, and H. Shaked, J. Appl. Phys. **83**, 6733 (1998).

[4] E. N. Caspi, H. Pinto, and M. Melamud, J. Appl. Phys. **87**, 416 (2000).

[5] K. Niihara and S. Yajima, Bull. Chem. Soc. Jpn. **46**, 770 (1973).

[6] P. Fischer, G. Frey, M. Koch, M. Könnecke, V. Pomjakushin, J. Schefer, R. Thut, N. Schlumpf, R. Bürge, U. Greuter, S. Bondt, and E. Berruyer, Physica B **276–278**, 146 (2000).

[7] J. R. Carvajal, Physica B **192**, 55 (1993).

[8] H. Ido, O. Nashima, T. Ito, T. Kaneda, Y. Saito, K. Konno, H. Yoshida, and M. Motokawa, J. Appl. Phys. **85**, 4865 (1999).

[9] J. S. Smart, *Effective Fields of Magnetism* (Saunders Company, Philadelphia & London, 1966) Chap. 11.

[10] W. Perthold, H. M. Hong, H. Michor, G. Hilscher, H. Ido, and H. Asano, J. Magn. Magn. Mater. **158**, 649 (1996).

[11] C. Piqué, R. Burriel, and J. Bartolomé., J. Magn. Magn. Mater. **154**, 71 (1996).

[12] The 16 NPD datasets were collected at the following temperatures: 1.5, 18.6, 26.9, 33.7, 39.4, 64.0, 83, 102, 122, 127, 132, 137, 142, 147, 149, 220 K.

[13] W. Opechowski and R. Guccione, in *Magnetism* edited by G. T. Rado and H. Suhl (Academic, New York, 1965), Vol. IIA, p. 105.

[14] E. Prince, Acta Crystallogr., Sect. B: Struct. Crystallogr. Cryst. Chem. **38**, 1099 (1982).

[15] H. Shaked, Physica B **353**, 310 (2004).

[16] C. Zlotea, C. Chacon, and O. Isnard, J. Appl. Phys. **92**, 7382 (2002).

[17] R. J. Radwański, J. Magn. Magn. Mater. **62**, 120 (1986).

[18] C. Rudowicz, J. Phys. C **18**, 1415 (1985).

[19] K. W. H. Stevens, Proc. Phys. Soc., London, Sect. A **65**, 209 (1952).

[20] J. E. Greedan and V. U. S. Rao, J. Solid State Chem. **6**, 387 (1973).

[21] H. H. A. Smit, R. C. Thiel, K. H. J. Buschow, J. Phys. F: Met. Phys. **18**, 295 (1988).

[22] M. Dubman, E. N. Caspi, E. Ettedgui, and H. Shaked, unpublished.

[23] K. N. Yang, M. S. Torikachvili, M. B. Maple, and H. C. Ku, J. Appl. Phys. **57**, 3140 (1985).

[24] E. N. Caspi, M. Dubman, H. Ettedgui, H. Shaked, S. Short, and J. D. Jorgensen, Physica B **359–361**, 944 (2005).

[25] R. Ballou, E. Burzo, and V. Pop, J. Magn. Magn. Mater. **140–144**, 945 (1995).

[26] V. V. Kelarev, V. V. Chuev, A. N. Pirogov, and S. K. Sidorov, Phys. Status Solidi A **79**, 57 (1983).

[27] A. C. Ermolenko, Yu. P. Irkhin, E. V. Rosenfeld, V. V. Kelarev, A. F. Rohzda, S. K. Sidorov, A. N. Pigorov, and A. P. Vokhmyanin, Zh. Eksp. Teor. Fiz. **69**, 1743 (1975).

[28] A. N. Pirogov, V. N. Dvinyaninov, V. V. Kelarev, V. V. Chuyev, and S. K. Sidorov, Phys. Met. Metallogr. **54**, 198 (1982).

[29] S. K. Malik, A. M. Umarji, and G. K. Shenoy, J. Appl. Phys. **57**, 3252 (1985).

[30] R. M. W. Strnat, in *Ferromagnetic Materials*, edited by E. P. Wohlfarth and K. H. J. Buschow (North-Holland, Amsterdam), Vol. 4, Chap. 2.

[31] T. Okamoto, H. Fujii, C. Inoue, and E. Tatsumoto, J. Phys. Soc. Jpn. **34**, 835 (1973).

[32] $\lambda^{\gamma,2}$ is the linear magnetostriction constant, calculated with substitution of the lattice parameters refined in the present work (Fig. 9). Notation and calculation follows: A. V. Andreev, in *Handbook of Magnetic Materials*, edited by K. H. J. Buschow (Elsevier North-Holland, New York, 1995), Vol. 8, Chap. 2.

[33] A. V. Andreev and S. M. Zadvorkin, Physica B **172**, 517 (1991).

[34] H. Ogata, H. Ido, and H. Yamauchi, J. Appl. Phys. **73**, 5911 (1993).

[35] N. H. Duc and D. Givord, J. Magn. Magn. Mater. **151**, L13 (1995).

[36] C. Chacon and O. Isnard, J. Phys.: Condens. Matter **13**, 5841 (2001).

[37] H. Yamada, K. Terao, H. Nakazawa, I. Kitagawa, N. Suzuki, and H. Ido, J. Magn. Magn. Mater. **183**, 94 (1998).

[38] R. L. Streever, Phys. Rev. B **19**, 2704 (1979).

[39] J. M. Alameda, D. Givord, R. Lemaire, and Q. Lu, J. Appl. Phys. **52**, 2079 (1981).

[40] J. Schweizer and F. Tasset, J. Phys. F: Met. Phys. **10**, 2799 (1980).

[41] K. Oda, K. Sugiyama, K. Kindo, N. M. Hong, H. Asano, O. Nashima, and H. Ido, J. Magn. Magn. Mater. **140–144**, 947 (1995).

[42] V. N. Syromyatnikov, A. N. Pigorov, V. V. Chuev, and V. V. Kelarev, Phys. Met. Metallogr. **52**, 80 (1981).